Longitudinal and Transversal Directed Overgrowth of Pentatwinned Silver Nanorods with Tunable Optical Properties

Claire Goldmann, Xiaoyan Li, Mathieu Kociak, Doru Constantin, Cyrille Hamon

Longitudinal and Transversal Directed Overgrowth of Pentatwinned Silver Nanorods with Tunable Optical Properties

Claire Goldmann,[1] Xiaoyan Li,[1] Mathieu Kociak,[1] Doru Constantin,[2] Cyrille Hamon[1]**

[1] Université Paris-Saclay, CNRS, Laboratoire de Physique des Solides, 91405 Orsay, France.

[2] Institut Charles Sadron, CNRS and Université de Strasbourg, 67034 Strasbourg, France.

KEYWORDS: seed-mediated growth; dimethyl sulfoxide; cathodoluminescence; SAXS; silver nanoparticles; EELS.

Abstract

Silver nanorods (AgNRs) with controllable aspect ratio can be formed by templated growth from pentatwinned seeds. However, it is challenging to control the volume of the AgNRs and their aspect ratio independently, due to the selective protection against growth of the lateral facets by halides. Here we demonstrate the preparation of AgNRs with tunable width via the addition of dimethyl sulfoxide (DMSO). AgNRs with custom dimensions were produced by separating the longitudinal and transverse growth in a two-step procedure. In the first step, the length is tuned by directing the overgrowth on the {111} tips of the AgNRs. In the second step, the width is adjusted by directing the overgrowth on the {100} lateral facets in the presence of DMSO. AgNRs of varying dimensions were obtained and characterized by a combination of techniques including scanning transmission electron microscopy, electron energy loss spectroscopy and cathodoluminescence, which are respectively sensitive to the extinction and scattering component of the AgNRs' response. This method allows tuning the plasmon energies, but also the ratio of the scattering and absorption contributions.

Table of Contents

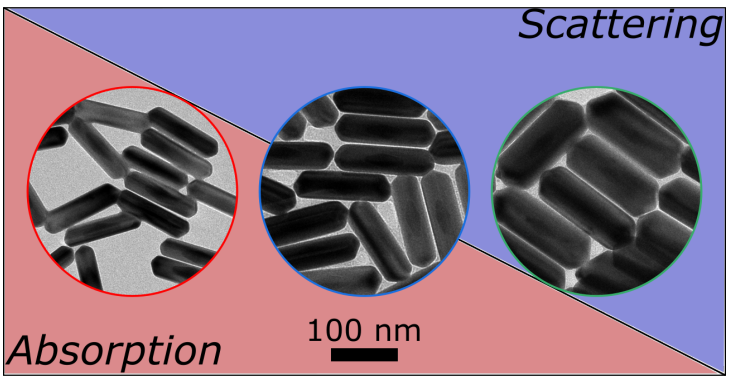

Introduction

Gold and silver nanoparticles have unique optical properties known as localized surface plasmon resonances (LSPR), originating from collective electron oscillations at optical frequencies.[1] The extinction spectrum includes both scattering and absorption components, which are strongly dependent on the particle morphology and size and on the local dielectric environment.[2] Anisotropic nanoparticles, such as nanorods, exhibit at least two different plasmon oscillations along the principal axes of the nanoparticle, known as transverse LSPR and longitudinal LSPR.[3-4] The longitudinal LSPR redshifts with increasing aspect ratio (length/width) and is tunable from the visible to the infrared region. Over the last 20 years, developments around LSPR and shape control of nanoparticles have become a cornerstone in research, with a great body of applications ranging from theranostics to sensing.[3, 5-10] Depending on the applications, either high absorption or scattering cross section are preferred, and can be achieved for small or large plasmonic nanorods respectively.[3-4] The ratio between scattering and extinction cross-sections scales linearly with the volume, while (for small nanoparticles) the energy of the plasmon scales to first order monotonically with the inverse of the aspect ratio. Despite significant advances, it is still challenging to control the volume of the plasmonic nanorods and their aspect ratio independently, which would be a key factor in controlling the amplitude of the response and the energy of the plasmons.

Among the different approaches for the preparation of plasmonic nanorods, seed-mediated growth methods consist in the rapid injection of small nanoparticles into a growth solution containing metal salt, as well as reducing, stabilizing and shape-directing agents.[11-12] For instance, monodisperse gold nanorods (AuNRs) and silver nanorods (AgNRs) with controllable aspect ratio can be formed by templated growth from pentatwinned seeds.[13-16] The crystallographic structure of the seeds contributes to the formation of the nanorods,[17] but stabilization of the {100} side facets by shape-directing agent such as Cl^- and ascorbic acid is

also essential for maintaining the shape over time.[13, 18] The metallic precursor deposits on the {111} facets at the tips, while the diameter of the nanorods remains almost constant over the growth process. Although the length of the nanorods can be well controlled by adjusting the amount of metallic precursors, the diameter can only be tuned by using seeds of different dimensions, resulting in very limited size control.

Some previous work intended to go beyond controlling the aspect ratio by also tailoring the length and width of nanorods. For instance, small thiolated molecules can be used to induce transversal growth by selectively capping the tips of AuNRs, but the conditions have to be carefully adjusted to avoid colloidal flocculation and unwanted shape evolution.[19-20] Great size tunability was achieved by disconnecting symmetry breaking and seeded growth of AuNRs,[21] yet this method only controls the aspect ratio of the nanorods and does not tune the length and width separately. It remains challenging to produce nanorods with tailored dimensions because of the high symmetry associated with the fcc lattice of Ag and Au. Moreover, aqueous approaches for the preparation of AgNRs in general lead to poor shape tunability compared to AuNRs. In a recent work, we have shown that dimethylsulfoxide (DMSO) at moderate concentration (i.e. 5% (v/v)), can be used to break the inversion symmetry of AgNRs by restricting growth to one end of a pentatwinned gold bipyramid seed.[22] Interestingly, at higher DMSO concentration (above 20% (v/v)), growth only occurred along the transverse axis of the seeds. We postulated that this procedure could be extended to control precisely the diameter of preformed AgNRs.

In this work, we produce AgNRs with custom dimensions by separating the longitudinal and transverse growth in a two-step procedure. In the first step, the length is tuned by directing the overgrowth on the {111} tips of the AgNRs. In the second step, the width is adjusted by directing the overgrowth on the {100} lateral facets in the presence of DMSO. The particle sizes are measured by a combination of transmission electron microscopy (TEM) imaging and

synchrotron-based small-angle X-ray scattering (SAXS). Combined scanning TEM (STEM) electron energy loss spectroscopy (EELS) and cathodoluminescence (CL) analysis show that this method allows tuning not only the LSPR energy, but also the scattering and extinction cross section of the AgNRs. This work is relevant for all applications that require fine-tuning of the optical properties of nanoparticles.

Experimental Section

Materials. Gold chloride trihydrate ($HAuCl_4 \cdot 3H_2O$ ≥99.9%), silver nitrate ($AgNO_3$ >99%), hydrochloric acid (HCl 37%), sodium borohydride ($NaBH_4$ ≥96%), trisodium citrate dihydrate (99%), L-ascorbic acid (AA ≥99%), anhydrous dimethylsulfoxyde (DMSO 99.9%), cetyltrimethylammonium bromide (CTAB ≥99%), CTAC (25 wt % in H_2O), and benzyldimethylhexadecylammonium chloride (BDAC 99%) were purchased from Merck and used without further purification.

Characterization of the NPs.

Extinction spectroscopy: UV/Vis/NIR absorption spectra were collected using a Cary 5000 UV-Vis-NIR. All experiments were carried out at room temperature, using disposable polystyrene cuvettes with optical paths of 1 cm. Gold concentration was estimated from the absorbance at 400 nm.[1, 2] TEM was performed at IMAGIF (I2BC CNRS, Gif s/Yvette, France) using a JEOL JEM-1400 microscope operating at 120 kV with a filament current of about 55 μA.

SAXS: SAXS measurements were performed on the SWING beamline of the SOLEIL synchrotron (Saint-Aubin, France) at a beam energy of E = 16 keV. The sample-to-detector distance was 6.22 m, covering a scattering vector range $0.0014 < q < 0.24$ Å^{-1}. The beam size was approximately 500×200 μm^2 (H × V). All measurements were performed at room temperature (22 °C).

The scattered signal was recorded by an Eiger 4 M detector (Dectris Ltd., Switzerland) with pixel size 75 μm. Preliminary data treatment (angular averaging and normalization) was done using the software Foxtrot developed at the beamline, which yielded the intensity as a function of the scattering vector I(q) in absolute units. Subsequent data modeling was done in Igor Pro 7.0 using specifically developed functions: the composite particles are described by a prolate ellipsoid (for the gold bipyramid core) with half-axes *a* and *b* contained within a circular cylinder (for the silver shell) of length *L* and diameter *D*. Polydispersity is accounted for by a homothetic Gaussian size distribution (affecting all dimensions similarly) with relative standard deviation *p*.

EELS/CL : The CL and EELS experiments were used to understand the optical extinction and scattering of the silver nanorods. They were performed on a modified NION Hermes200 monochromated and Cs-corrected Scanning transmission electron microscope. CL detection used a Mönch system from Attolight, fitted with a diffraction grating given an energy resolution of 4meV. EELS detection used a MerlinEM direct electron detector from Quantum DETECTORS. In this work, the experiments were operated at 60keV, at a typical condenser convergent angle of 10mrad, a typical EELS energy resolution of 20 meV and a CL spectral range from 325 to 870 nm.

Boundary Element Method (BEM) simulation details: Simulated extinction spectra were calculated by the boundary element method (BEM), using the MNPBEM toolbox developed in the MATLAB environment.[3] The GBPs are described as a gold bicone with 33.2 nm in length and 14.9 nm in base-width, terminated with two spherical caps. The silver shell is described as a spherocylinder with the coresponding mean width and length determined by size distribution analysis. Simulations were performed to solve the full Maxwell's equations (including retardation effects). The dielectric properties of gold and silver were taken from P. B. Johnson

and R. W. Christy.[4] We used an arbitrary value for the dielectric constant (i.e. 1.33) in order to take into account the Si_3N_4 membrane/NPs interaction.

Bipyramids synthesis and purification

Seeds. In a 50 mL bottle, 2.65 mL of CTAC (25 wt % in H_2O) and 400 µL of $HAuCl_4$ 25 mM were mixed to 33 mL of water and heated at 30°C for 10 minutes. 4 mL of sodium citrate 50 mM were added and the heating was continued for 30 minutes. Under fast stirring, 1 mL of $NaBH_4$ 25 mM was added, then the bottle was closed and put in the oven at 40°C for 5 days.

Growth. 500 µL of $AgNO_3$ (100 mM), 10 mL of $HAuCl_4$ (25 mM), and 10 mL of HCl (1 M) were added in 500 mL of CTAB (100 mM). Then, 4 mL of AA (100 mM) was added, followed by 7.5 mL of seeds (15 mL for smaller BPs). After 4 h at 30 °C, the bipyramids were centrifuged twice and purified by depletion induced flocculation during one night at 30 °C in BDAC (350 mM).[5] The supernatant was removed, and the precipitate was redispersed in water and washed twice with 10 mM CTAC. The AuBPs were finally redispersed in 1 mL of 10 mM CTAC. For small BPs (i.e. batch 3, Figure S1), the purification is not possible, the particles were only centrifuged and washed with CTAC 10 mM.

Silver growth on the gold bipyramids. In a vial, water, CTAC and AuBPs were mixed and heated at 70°C for 5 minutes. Under strong stirring, silver nitrate was added, followed by ascorbic acid, the vial was closed and the reaction medium was heated for 2 hours at 70°C (see table S1 for precise quantities). After being cooled at room temperature, the UV/Vis/NIR absorption spectra of the suspension was recorded, using typically 100-150 µL of reaction medium and 3000 µL of water. The particles were centrifuged, washed and stored in 2 mL of CTAC 1 mM (named here after "stock solution").

In a second growth step, 10 µL of stock solution were diluted in 2000 µL of water and their UV-visible spectrum was recorded. As there is no straightforward relation between the

absorbance and the gold concentration for such composite nanoparticles, the concentration was determined using the expected concentration of the stock solution (considering that every bipyramid seed formed one Ag rod). Consequently, it is very important to know precisely the reaction medium volume (and the initial Au(0) concentration), to close well vials to avoid evaporation, and to keep a record of every dilution used in the preparation of the samples.

Silver growth on the {111} facets / growth in length. In a vial, water, CTAC and Au@AgNRs were mixed and heated at 70°C for 5 minutes. Under strong stirring, silver nitrate was added, followed by ascorbic acid, the vial was closed and the reaction medium was heated for 2 hours at 70°C (see table S2 for precise quantities). After being cooled at room temperature, the UV/Vis/NIR absorption spectra of the suspension was recorded, using typically 100-150 µL of reaction medium and 3000 µL of water. The particles were centrifuged, washed and stored in CTAC 1 mM.

Silver growth on the {100} facets / growth in width. In a vial, water, CTAC, DMSO and AuBPs were mixed and heated at 70°C for 20 minutes. Under strong stirring, silver nitrate was added, followed by ascorbic acid, the vial was closed and the reaction medium was heated for 2 hours at 70°C (see table S3 for precise quantities). After being cooled at room temperature, the UV/Vis/NIR absorption spectra of the suspension was recorded, using typically 100-150 µL of reaction medium and 3000 µL of water. The particles were centrifuged, washed and stored in CTAC 1 mM.

Result and discussion

Gold bipyramids were prepared with a high shape yield, as recently reported.[23-24] AgNRs were formed by directed growth along the fivefold axis of the bipyramids in an aqueous mixture containing hexadecyltrimethylammonium chloride (CTAC) and ascorbic acid (AA) and heated at 70°C.[14] In these conditions, AgNRs 120±4.9 nm in length and 28.2 ±1.4 nm in

width were obtained. The AgNRs were overgrown a second time with a fresh growth solution, either of the same composition (0% DMSO) or with 20% DMSO, keeping the other experimental parameters fixed. The silver-to-gold molar ratio K (Ag ions per Au atoms in the nanorods) was varied up to K=20 and the shape of the resulting AgNRs was investigated by TEM (Figure 1A-B) and SAXS (see the Supporting Information).

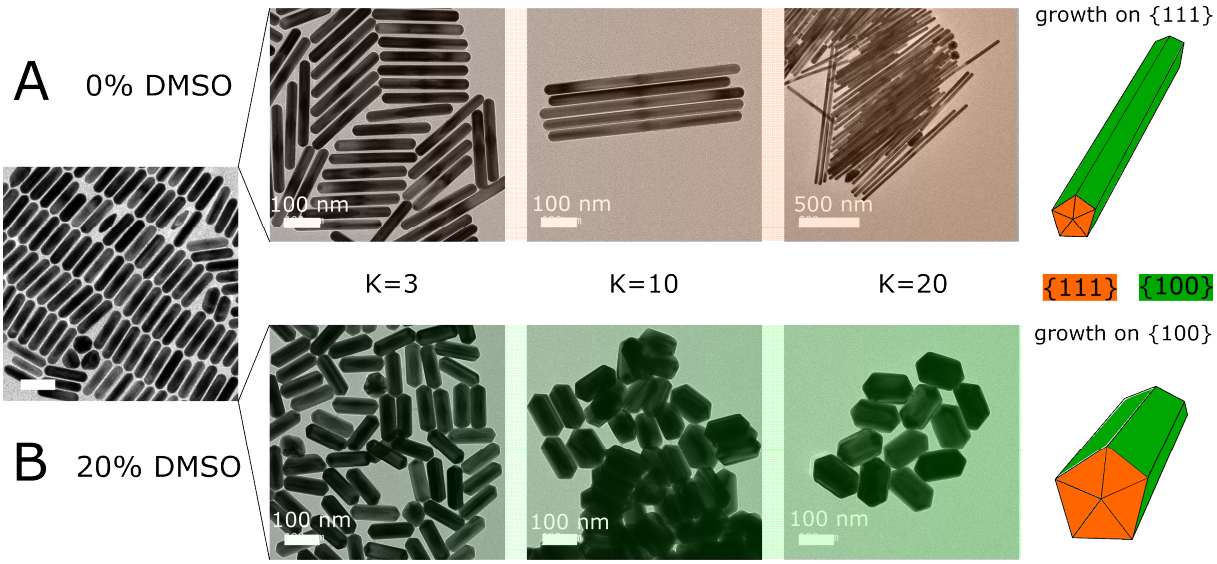

Figure 1: Representative TEM images of AgNRs obtained in the presence or in the absence of DMSO. AgNRs 120±4.9 nm in length and 28.2 ±1.4 nm in width were used as seeds for subsequent overgrowth, either with 0% DMSO (A) or with 20 % DMSO (B). AgNRs were overgrown with varying K (i.e. silver-to-gold molar ratio).

At 0% DMSO and 20% DMSO, the rods grew either in the longitudinal or in the transverse direction respectively, and marked differences can be observed between the two types of rods at K=20. Pentatwinned nanorods are known to display two families of facets: five {100} lateral facets and five {111} facets at each tips.[25-26] At 0% DMSO, the silver ions deposited preferentially along the {111} facets, resulting in an elongation of the AgNRs (Figure 1A). However, at 20% DMSO the rods thicken but do not elongate, as the growth takes place preferentially on the {100} facets (Figure 1B). Note that, in both cases, the growth occurs at the

same rate on the two families of facets because the gold core remains at the center of mass of the AgNR after synthesis, unlike the case of intermediate DMSO concentration, where asymmetric growth can occur.[22] Previous MD simulations have shown that DMSO can deform CTAC micelles and replace the capping Cl^- ion (which is known to stabilize the {100} facets[18]) by binding at the surface of gold nanoparticles.[22] Our results suggest that DMSO competes with the chemisorption of halides, leading to a decrease in the surface energy of the {111} tip facets, and thus to an increase in their size.

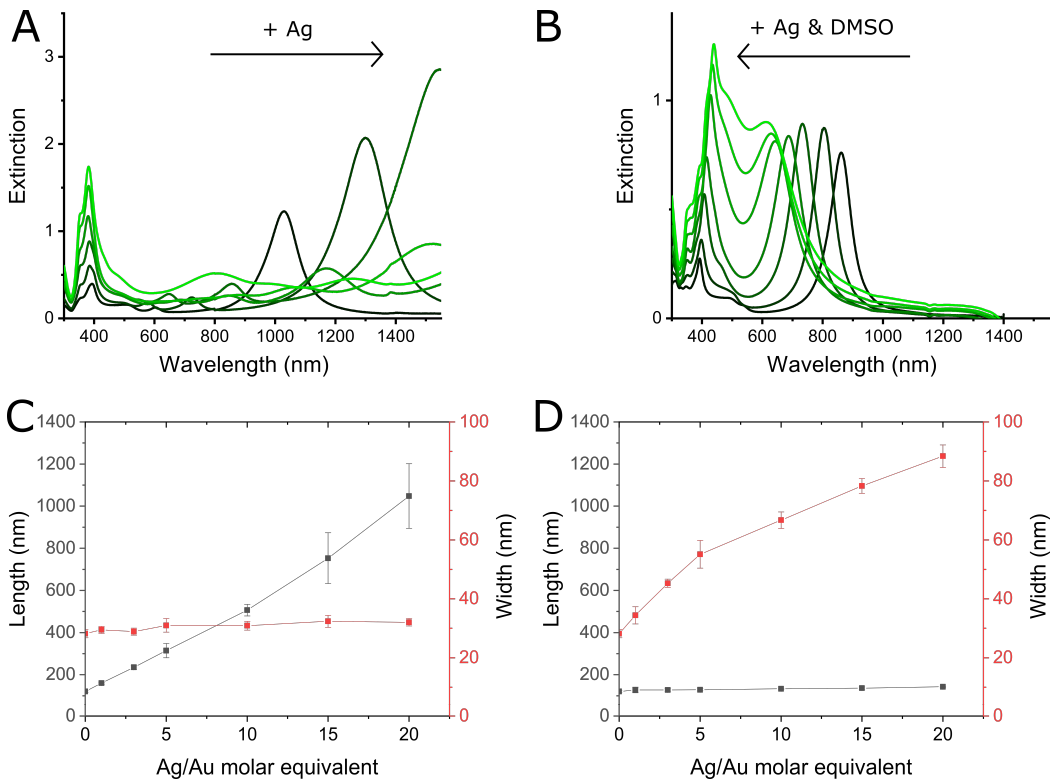

Figure 2: Silver nanorods with tunable dimensions and optical properties. A-B) Extinction spectra of Ag rods (120±4.9 nm in length and 28.2 ±1.4 nm in width) overgrown without DMSO (A) and with 20 % DMSO (B). K was varied between 1-20. Size (length and width) evolution obtained from the TEM image analysis of Ag rods for different Ag/Au molar equivalent with no DMSO (C) and with DMSO (D). Symbols and error bars represent mean values and standard deviations.

Extinction spectroscopy and TEM size distribution analysis show a marked difference in the overgrowth performed with 0% (v/v) and 20 % (v/v) DMSO. At 0% DMSO, the longitudinal LSPR constantly red-shifted upon increasing the Ag/Au molar equivalent as a direct consequence of the increase in aspect ratio of the nanorods (Figure 2A). Corresponding size distribution analysis revealed a linear relationship between the length of the nanorods and K, while the width remained constant (Figure 2B). At K=10, AgNRs of 506.5±27.5 (mean±SD) nm in length and 30.9±1.5 nm in width were obtained, corresponding to a size increase relative to the AgNRs seeds of 321% in length and 9.6% in width. In contrast, at 20% DMSO, AgNRs of 132.6±2.9 nm in length and 66.7±2.8 nm in width were obtained keeping the other experimental parameters fixed (Figure 2D). The corresponding relative size increase to the AgNRs seeds of 9.5% in length and 58% in width resulted in a decrease of the aspect ratio of the AgNRs and a blue shift of the longitudinal LSPR (Figure 2B). The size distribution analysis revealed a linear relationship between the width of the nanorods and K with a change in slope around K=5, which can be explained by the enlargement of the {111} facets at the tips of the pentatwinned rods.

Next, we combined {111} and {100} directed growth to obtain AgNRs with tunable dimension in a two-steps process that is schematized in a synthetic flowchart in Figure 3A.

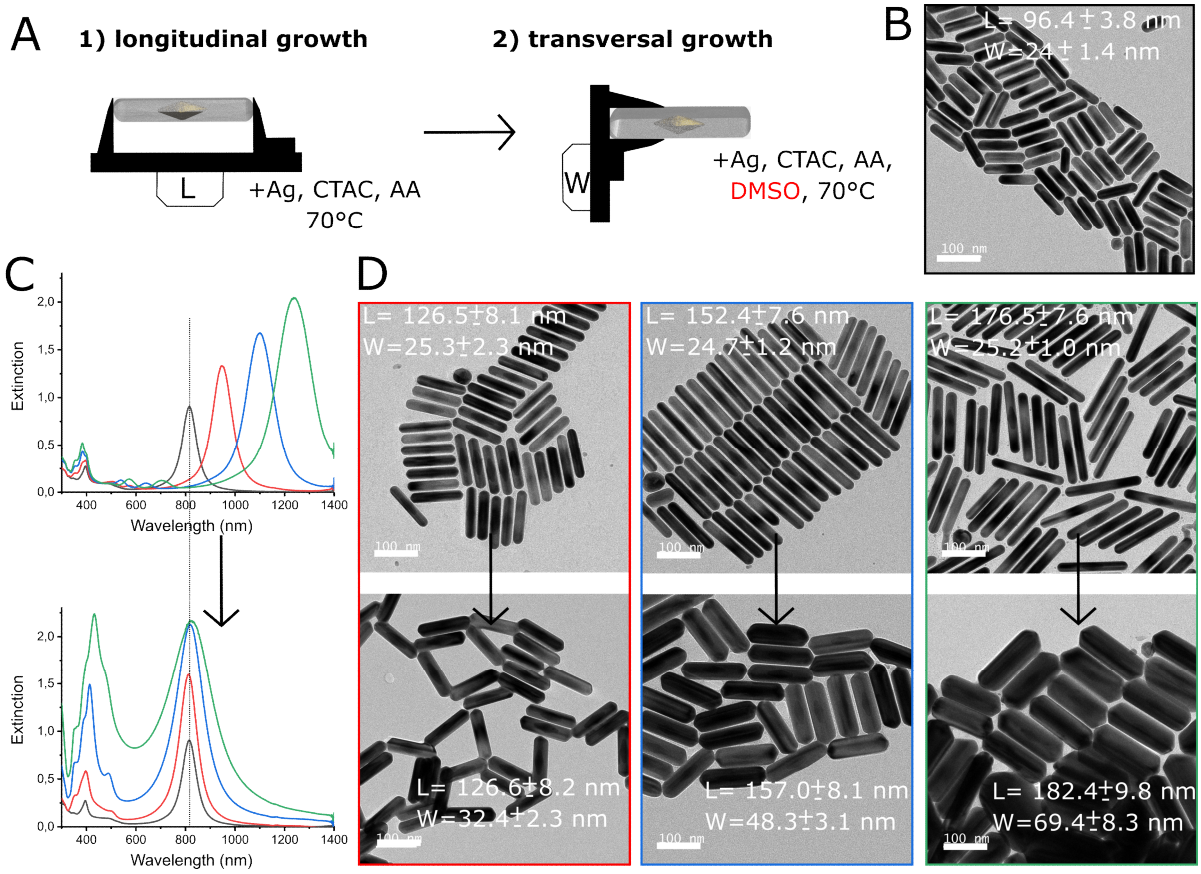

Figure 3: Two-step process for the preparation of AgNRs with custom dimensions and optical properties. A) Schematic flowchart of the two-step process. In the first step, AgNR seeds are overgrown in the longitudinal direction. In the second step, the particles are overgrown in the transverse direction. B) TEM image of the AgNR seeds. C) Extinction spectra of four nanorod batches of varying dimensions. The black trace corresponds to the AgNR seed. (top) the samples have varying lengths and about the same widths. (bottom) the samples are overgrown in the transverse direction so that the LSPR matches the one of the AgNR seeds (black). D) TEM images of AgNRs before and after transverse overgrowth. Scale bar on all images is 100 nm. Size distribution analysis for AgNRs are indicated on the corresponding TEM image.

As a proof of concept, we prepared AgNRs with different volumes but similar aspect ratios, in order to fix the LSPRs at the same energy. First, the longitudinal growth is performed without DMSO followed by a second overgrowth in the presence of DMSO to adjust the width of the

AgNRs (Figure 3). Three AgNR batches were prepared, with a width of about 25 nm and various lengths (126, 152 and 176 nm) corresponding to a longitudinal LSPR of 946, 1100 and 1236 nm respectively. Then, overgrowth was performed in presence of DMSO and the longitudinal LSPR was tracked as a function of K, until it matched the longitudinal LSPR of the AgNR seeds at 815 nm (Figure S4). This experiment resulted in four batches of AgNRs with the same SPR energies but with different dimensions.

We then analyzed the extinction and scattering characteristics of these AgNRs at the single particle level by STEM-EELS and CL. Indeed, in the case of nanoparticles, it has been proven than these techniques can be viewed as nanometer-scale counterparts of extinction and scattering spectroscopy, respectively.[27] We performed the experiments at 60 kV accelerating voltage with a Hermes 200 kV NION microscope fitted with the Attolight Mönch cathodoluminescence detector. We prepared two new batches of AgNRs with the longitudinal LSPR centered around 680 nm, within the 325-870 nm spectral range accessible with our CL setup.

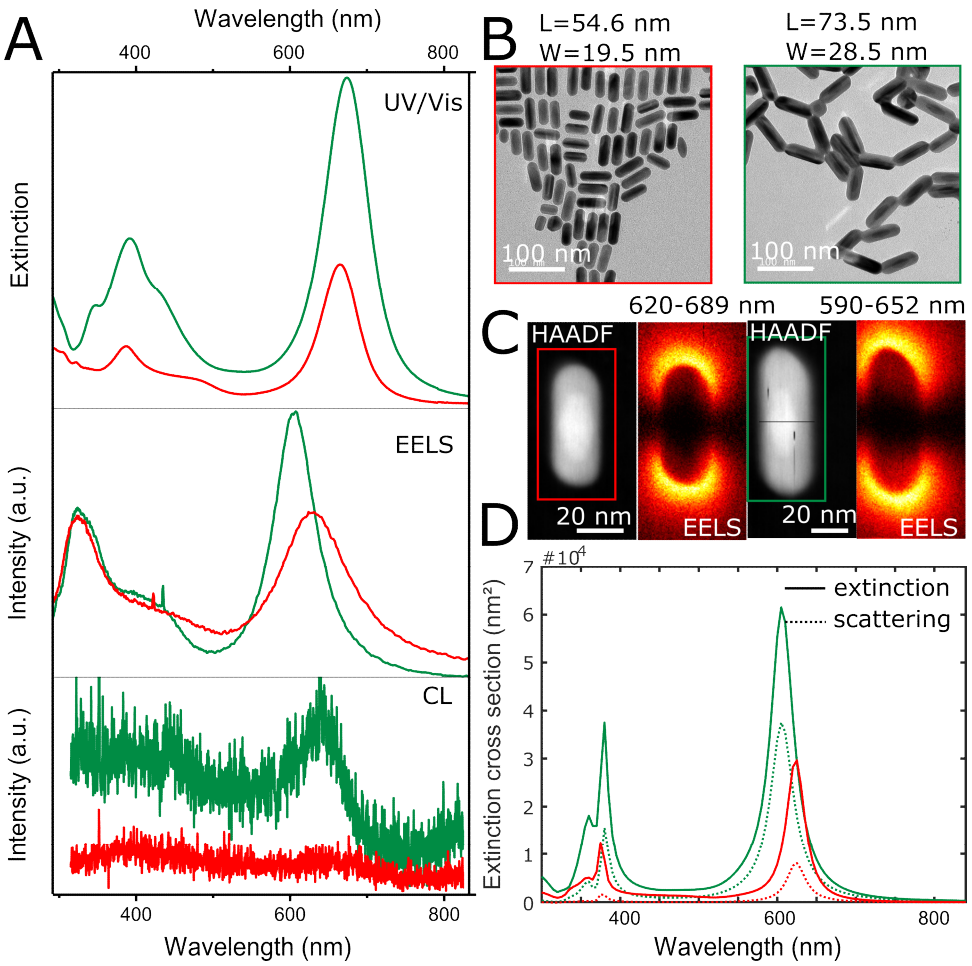

Figure 4: Comparison of the optical properties of two types of AgNRs with different volumes and similar aspect ratio. A) UV/Vis (top), STEM-EELS (middle), CL (bottom) of the small (red, 54.6±4.4 nm in length and 19.5±0.94 nm in width) and large AgNRs (green, 73.5±4.3 nm in length and 28.5±1.74 nm in width). B) Representative TEM images of the two nanorod batches. C) STEM-HAADF images of the two AgNRs measured in EELS and CL and corresponding EELS filter maps of the dipolar mode. The colored box indicates the region over which the EELS and CL spectra were taken. D) Numerical BEM simulations of the extinction spectra (solid line) of the small (red) and large AgNRs (green), including the scattering contribution (dashed line).

At the ensemble and single particle level, the optical properties of the small and large AgNRs were similar, although the position of the longitudinal LSPR was blue-shifted compared to the

ensemble measurement due to the change in dielectric environment. The shift is not exactly the same for the two AgNRs that can be due to multiple factors, including the slight difference between the average dimensions of a given sample as measured in extinction experiment with the dimension of the peculiar nanorod investigated in EELS. Note that the extinction cross section of the large rods was always higher than for the small rods, as a direct consequence of their higher volume. A shift of the LSPR position of 35 nm was noted between EELS and CL experiments. Shifts with similar if not higher values have been reported both in gold and silver nanoparticles.[27-28] In this works, the reported shifts were related to energy dependent specificities of the dielectric constants of the nanoparticles and/or their substrates, although the order of magnitude of the shifts were not completely explained. Recently, it was demonstrated that the exact CL peak position could be modified by the collection geometry.[29] Moreover, only the signal of the large rods could be detected in CL. This result can be explained by the higher scattering cross-section of the large rods compared to the small rods that are thus more radiative, which validate our approach. We then performed retarded electromagnetic simulations by the boundary element method (BEM)[30] to determine the respective radiative (scattering) and non-radiative (absorption) contribution of both types of rods to the extinction cross section (Figure 4D). As expected, the balance between scattering and absorption varied significantly in this size range, explaining the signal intensities measured experimentally.

Conclusions

A simple and robust approach to control independently the dimensions (length and width) of AgNRs was demonstrated in a two-step process. In the first step, longitudinal growth was achieved in an aqueous reaction medium. In the second step, the growth was inhibited at the tips and promoted on the sides by the addition of 20% DMSO in the reaction mixture. We explain this phenomenon by the selective capping of the {100} lateral facets by Cl^- in the first step, whereas capping of the {111} tip facets by DMSO is responsible for transversal growth

in the second step. Our methodology allows controlling the radiative (scattering) and nonradiative (absorbing) contributions of the AgNRs at a fixed wavelength by adjusting their volume. This strategy is promising for applications that require nanoobjects with controlled absorbing (e.g. photothermia) and radiative (e.g. imaging based on light scattering) properties.

Supporting Information

Details about synthesis and additional extinction spectroscopy, SAXS, TEM, EELS, CL data. This material is available free of charge via the Internet at http://pubs.acs.org.

Author information

Corresponding authors

***E-mail:** constantin@unistra.fr

***E-mail:** cyrille.hamon@universite-paris-saclay.fr

Acknowledgements

The present work has benefited from the electronic microscopy facility of Imagerie-Gif, (http://www.i2bc.parissaclay.fr), member of IBiSA (http://www.ibisa.net), supported by "France-BioImaging" (ANR-10-INBS-04-01), and the Labex "Saclay Plant Science" (ANR-11-IDEX-0003-02). This work has received support from the French State through the National Agency for Research under the program of future investment EQUIPEX TEMPOS-CHROMATEM with the reference ANR-10-EQPX-50. We acknowledge SOLEIL for the provision of synchrotron radiation facilities and we would like to thank Thomas Bizien for assistance in using beamline SWING.

References

1. Liz-Marzán, L. M. Nanometals: Formation and color. *Mater. Today* **2004,** *7* (2), 26-31.

2. Link, S.; El-Sayed, M. A. Spectral Properties and Relaxation Dynamics of Surface Plasmon Electronic Oscillations in Gold and Silver Nanodots and Nanorods. *J. Phys. Chem. B* **1999,** *103* (40), 8410-8426.

3. Zheng, J.; Cheng, X.; Zhang, H.; Bai, X.; Ai, R.; Shao, L.; Wang, J. Gold Nanorods: The Most Versatile Plasmonic Nanoparticles. *Chem. Rev.* **2021,** *121* (21), 13342-13453.

4. Chen, H.; Shao, L.; Li, Q.; Wang, J. Gold nanorods and their plasmonic properties. *Chem. Soc. Rev.* **2013,** *42* (7), 2679-2724.

5. Chen, Y.-S.; Zhao, Y.; Yoon, S. J.; Gambhir, S. S.; Emelianov, S. Miniature gold nanorods for photoacoustic molecular imaging in the second near-infrared optical window. *Nat. Nanotechnol.* **2019,** *14* (5), 465-472.

6. Wang, H.; Huff, T. B.; Zweifel, D. A.; He, W.; Low, P. S.; Wei, A.; Cheng, J.-X. In vitro and in vivo two-photon luminescence imaging of single gold nanorods. Proc. Natl. Acad. Sci. U. S. A **2005,** *102* (44), 15752-15756.

7. Durr, N. J.; Larson, T.; Smith, D. K.; Korgel, B. A.; Sokolov, K.; Ben-Yakar, A. Two-Photon Luminescence Imaging of Cancer Cells Using Molecularly Targeted Gold Nanorods. *Nano Lett.* **2007,** *7* (4), 941-945.

8. Huang, X.; El-Sayed, I. H.; Qian, W.; El-Sayed, M. A. Cancer Cells Assemble and Align Gold Nanorods Conjugated to Antibodies to Produce Highly Enhanced, Sharp, and Polarized Surface Raman Spectra: A Potential Cancer Diagnostic Marker. *Nano Lett.* **2007,** *7* (6), 1591-1597.

9. Alvarez-Puebla, R. A.; Agarwal, A.; Manna, P.; Khanal, B. P.; Aldeanueva-Potel, P.; Carbó-Argibay, E.; Pazos-Pérez, N.; Vigderman, L.; Zubarev, E. R.; Kotov, N. A. et al. Gold nanorods 3D-supercrystals as surface enhanced Raman scattering spectroscopy substrates for the rapid detection of scrambled prions. Proc. Natl. Acad. Sci. U. S. A **2011,** *108* (20), 8157-8161.

10. Dreaden, E. C.; Alkilany, A. M.; Huang, X.; Murphy, C. J.; El-Sayed, M. A. The golden age: gold nanoparticles for biomedicine. *Chem. Soc. Rev.* **2012,** *41* (7), 2740-2779.

11. Xia, Y.; Gilroy, K. D.; Peng, H. C.; Xia, X. Seed-Mediated Growth of Colloidal Metal Nanocrystals. *Angew. Chem. Int. Ed.* **2017,** *56* (1), 60-95.

12. Haidar, I.; Day, A.; Decorse, P.; Lau-Truong, S.; Chevillot-Biraud, A.; Aubard, J.; Félidj, N.; Boubekeur-Lecaque, L. Tailoring the Shape of Anisotropic Core–Shell Au–Ag Nanoparticles in Dimethyl Sulfoxide. *Chem. Mater.* **2019,** *31* (8), 2741-2749.

13. Aliyah, K.; Lyu, J.; Goldmann, C.; Bizien, T.; Hamon, C.; Alloyeau, D.; Constantin, D. Real-Time In Situ Observations Reveal a Double Role for Ascorbic Acid in the Anisotropic Growth of Silver on Gold. *J. Phys. Chem. Lett.* **2020,** *11* (8), 2830-2837.

14. Zhuo, X.; Zhu, X.; Li, Q.; Yang, Z.; Wang, J. Gold Nanobipyramid-Directed Growth of Length-Variable Silver Nanorods with Multipolar Plasmon Resonances. *ACS Nano* **2015,** *9* (7), 7523-35.

15. Khanal, B. P.; Zubarev, E. R. Chemical Transformation of Nanorods to Nanowires: Reversible Growth and Dissolution of Anisotropic Gold Nanostructures. *ACS Nano* **2019,** *13* (2), 2370-2378.

16. Mayer, M.; Scarabelli, L.; March, K.; Altantzis, T.; Tebbe, M.; Kociak, M.; Bals, S.; García de Abajo, F. J.; Fery, A.; Liz-Marzán, L. M. Controlled Living Nanowire Growth: Precise Control over the Morphology and Optical Properties of AgAuAg Bimetallic Nanowires. *Nano Lett.* **2015,** *15* (8), 5427-5437.

17. Lofton, C.; Sigmund, W. Mechanisms Controlling Crystal Habits of Gold and Silver Colloids. *Adv. Funct. Mater.* **2005,** *15* (7), 1197-1208.

18. Gómez-Graña, S.; Goris, B.; Altantzis, T.; Fernández-López, C.; Carbó-Argibay, E.; Guerrero-Martínez, A.; Almora-Barrios, N.; López, N.; Pastoriza-Santos, I.; Pérez-Juste, J.; et al. Au@Ag Nanoparticles: Halides Stabilize {100} Facets. *J. Phys. Chem. Lett.* **2013,** *4* (13), 2209-2216.

19. Kou, X.; Zhang, S.; Yang, Z.; Tsung, C.-K.; Stucky, G. D.; Sun, L.; Wang, J.; Yan, C. Glutathione- and Cysteine-Induced Transverse Overgrowth on Gold Nanorods. *J. Am. Chem. Soc.* **2007,** *129* (20), 6402-6404.

20. Ni, W.; Kou, X.; Yang, Z.; Wang, J. Tailoring Longitudinal Surface Plasmon Wavelengths, Scattering and Absorption Cross Sections of Gold Nanorods. *ACS Nano* **2008,** *2* (4), 677-686.

21. González-Rubio, G.; Kumar, V.; Llombart, P.; Díaz-Núñez, P.; Bladt, E.; Altantzis, T.; Bals, S.; Peña-Rodríguez, O.; Noya, E. G.; MacDowell, L. G.; et al Disconnecting Symmetry Breaking from Seeded Growth for the Reproducible Synthesis of High Quality Gold Nanorods. *ACS Nano* **2019,** *13* (4), 4424-4435.

22. Goldmann, C.; De Frutos, M.; Hill, E. H.; Constantin, D.; Hamon, C. Symmetry Breaking in Seed-Mediated Silver Nanorod Growth Induced by Dimethyl Sulfoxide. *Chem. Mater.* **2021,** *33* (8), 2948-2956.

23. Sanchez-Iglesias, A.; Winckelmans, N.; Altantzis, T.; Bals, S.; Grzelczak, M.; Liz-Marzan, L. M. High-Yield Seeded Growth of Monodisperse Pentatwinned Gold Nanoparticles through Thermally Induced Seed Twinning. *J. Am. Chem. Soc.* **2017,** *139* (1), 107-110.

24. Chateau, D.; Liotta, A.; Vadcard, F.; Navarro, J. R.; Chaput, F.; Lerme, J.; Lerouge, F.; Parola, S. From gold nanobipyramids to nanojavelins for a precise tuning of the plasmon resonance to the infrared wavelengths: experimental and theoretical aspects. *Nanoscale* **2015,** *7* (5), 1934-43.

25. Johnson, C. J.; Dujardin, E.; Davis, S. A.; Murphy, C. J.; Mann, S. Growth and form of gold nanorods prepared by seed-mediated, surfactant-directed synthesis. *J. Mater. Chem.* **2002,** *12* (6), 1765-1770.

26. Sun, Y.; Mayers, B.; Herricks, T.; Xia, Y. Polyol Synthesis of Uniform Silver Nanowires: A Plausible Growth Mechanism and the Supporting Evidence. *Nano Lett.* **2003,** *3* (7), 955-960.

27. Losquin, A.; Zagonel, L. F.; Myroshnychenko, V.; Rodríguez-González, B.; Tencé, M.; Scarabelli, L.; Förstner, J.; Liz-Marzán, L. M.; García de Abajo, F. J.; Stéphan, O. et al. Unveiling Nanometer Scale Extinction and Scattering Phenomena through Combined Electron

Energy Loss Spectroscopy and Cathodoluminescence Measurements. *Nano Lett.* **2015,** *15* (2), 1229-1237.

28. Kawasaki, N.; Meuret, S.; Weil, R.; Lourenço-Martins, H.; Stéphan, O.; Kociak, M. Extinction and Scattering Properties of High-Order Surface Plasmon Modes in Silver Nanoparticles Probed by Combined Spatially Resolved Electron Energy Loss Spectroscopy and Cathodoluminescence. *ACS Photonics* **2016,** *3* (9), 1654-1661.

29. Schmidt, F.-P.; Losquin, A.; Horák, M.; Hohenester, U.; Stöger-Pollach, M.; Krenn, J. R. Fundamental Limit of Plasmonic Cathodoluminescence. *Nano Lett.* **2021,** *21* (1), 590-596.

30. Hohenester, U.; Trügler, A. MNPBEM – A Matlab toolbox for the simulation of plasmonic nanoparticles. *Comput. Phys. Commun.* **2012,** *183* (2), 370-381.